Signal, Image and Video Processing (2022) 16:931–936
https://doi.org/10.1007/s11760-021-02037-7

ORIGINAL PAPER

Optimal harvesting and sensing durations for multi-antenna cognitive radio networks using intelligent reflecting surfaces

Raed Alhamad[1]

Received: 3 July 2021 / Revised: 14 September 2021 / Accepted: 17 September 2021 / Published online: 28 October 2021

Abstract

In this paper, we suggest to optimize harvesting and sensing duration for cognitive radio networks (CRN) using intelligent reflecting surfaces (IRS). The secondary source S_S harvests energy using the signal of node A. Then, S_S performs spectrum sensing to detect primary source P_S activity. When P_S activity is not detected, S_S transmits a packet to secondary destination S_D. IRS reflects the signals from the secondary source so that all reflections are in phase at secondary destination. We show that the use of N=8,16,32,64,128, 256,512 reflectors offers 19, 25, 31, 37, 43, 49, 56 dB gain when compared to the absence of IRS [20]. We also propose to add a second IRS between node A and S_S to increase the harvested energy since S_S harvests energy using the reflected signals on the first IRS. The use of two IRS with $N_1 = 8$ reflectors in the first IRS and $N_2 = 8$ reflectors in the second IRS offers 12 dB and 30 dB gain when compared to a single IRS $N = 8$ and the absence of IRS [20]. The use of two IRS with $N_1 = 16$ and $N_2 = 8$ offers 21 dB and 39 dB gain when compared to a single IRS $N = 8$ and the absence of IRS [20].

Keywords Intelligent reflecting surfaces · Cognitive radio · Optimal harvesting · Optimal sensing · Throughput maximization

1 Introduction

In CRN, primary and secondary users (PU and SU) share the same spectrum. In interweave CRN, secondary source transmits when primary source is idle. In underlay CRN, secondary source transmits with an adaptive transmit power to generate low interference at secondary destination. In overlay CRN, secondary source dedicates a part of its power to help the secondary destination in decoding its packet. In this paper, we optimize harvesting and sensing durations for interweave CRN using intelligent reflecting surfaces (IRSs). IRSs allow an increase in the throughput of wireless networks since the reflected signals are in phase at the destination [1–5]. IRS is placed between the source and the destination with optimized phase shifts so that all reflections are in phase at the destination [6,7]. IRS has been suggested for wireless networks as well as non- orthogonal multiple access (NOMA) [8,9]. IRSs have been used to increase the throughput of optical communications as well as millimeter wave communications [10–12]. IRS with finite phase shifts has been suggested in [13]. Asymptotic performance analysis of wireless communications using IRS was provided in [14]. Antenna design, simulations and measurements of wireless communication using IRS were discussed in [15–17]. Machine and deep learning algorithms were used to optimize IRS implementation [18,19]. IRSs are nearly passive devices, made of electromagnetic material that can be deployed in primary or secondary networks of CRN on several structures, including but not limited to building facades, indoor walls, aerial platforms, roadside billboards, vehicle windows, etc.

In this article, we optimize harvesting and sensing duration for CRN using IRS. The secondary source S_S harvests energy using the signal of node A. Then, S_S performs spectrum sensing to detect the activity of P_S. When P_S activity is not detected, S_S transmits a packet to secondary destination S_D. The transmitted signal by S_S is reflected by N reflectors of IRS so that all reflections are in phase at S_D. We show that the use of $N = 8, 16, 32, 64, 128, 256, 512$ reflectors offers 19, 25, 31, 37, 43, 49, 56 dB gain when compared to the absence of IRS [20]. We also propose to add a second IRS between node A and S_S to increase the harvested energy since S_S harvests energy using the reflected signals on the

✉ Raed Alhamad
ralhamad@seu.edu.sa

[1] College of Computation and Informatics, Information Technology Department, Saudi Electronic University, Riyadh, Saudi Arabia

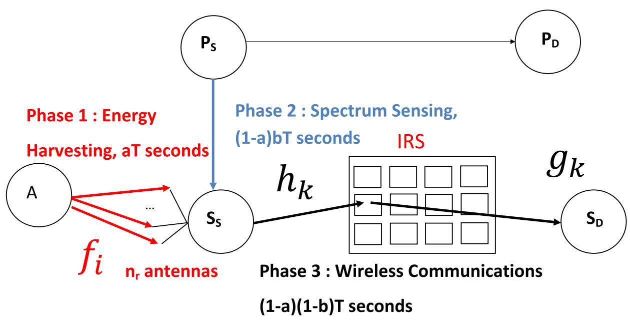

Fig. 1 CRN using a single IRS

first IRS. The use of two IRS with $N_1 = 8$ reflectors in the first IRS and $N_2 = 8$ reflectors in the second IRS offers 12 dB and 30 dB gain when compared to a single IRS $N = 8$ and the absence of IRS [20]. The use of two IRS with $N_1 = 16$ and $N_2 = 8$ offers 21 dB and 39 dB gain when compared to a single IRS $N = 8$ and the absence of IRS [20]. IRS with adaptive transmit power was studied in [21].

Next section derives the throughput when there is a single IRS. Section 3 proposes to add a second IRS to increase the harvested energy. Section 4 shows the throughput enhancement using a single or two IRS. Conclusions and perspectives are presented in Sect. 5.

2 CRN with one IRS

Figure 1 depicts the system model with a secondary source (S_S) equipped with n_r receive antennas used to harvest energy over aT seconds using the signal of node A. $0 < a < 1$ is the harvesting percentage and T is the frame duration. S_S performs spectrum sensing to detect primary source P_S activity during $(1-a)bT$ seconds where $0 < b < 1$ provides the sensing duration. When P_s activity is not detected, S_S transmits data to secondary destination S_D over $(1-b)(1-a)T$ seconds. The transmitter signal is reflected on IRS equipped with N reflectors so that all reflections are in phase at S_D. A Rayleigh fading channel is used during the simulations.

The harvested energy at S_S is expressed as

$$E = \mu a T P_A \sum_{l=1}^{n_r} |f_l|^2 = \mu a L_0 E_A \sum_{l=1}^{n_r} |f_l|^2, \quad (1)$$

where μ is the efficiency of energy conversion, $P_A = \frac{E_A}{T_s}$ is the power of A, T_s **is the symbol period,** $L_0 = \frac{T}{T_s}$. The average power of channel gain f_l between A and l-th antenna of S_S is $E(|f_l|^2) = \frac{1}{D_1^{ple}}$ where $E(X)$ is the expectation of X, D_1 is the distance between A and S_S, and ple is the path loss exponent.

The symbol energy of S_S is computed as

$$E_{S_S} = \frac{E}{L_0(1-a)(1-b)} = \frac{\mu a E_A}{(1-a)(1-b)} \sum_{l=1}^{n_r} |f_l|^2. \quad (2)$$

Let h_q be the channel gain between S_S and q-th reflector of IRS. Let g_q be the channel gain between q-th reflector of IRS and S_D. h_q follows a zero mean Gaussian distribution with $E(|h_q|^2) = \frac{1}{D_2^{ple}}$ where D_2 is the distance between S_S and IRS. g_q follows a zero-mean Gaussian distribution with $E(|g_q|^2) = \frac{1}{D_3^{ple}}$ where D_3 is the distance between IRS and S_D.

We have $h_q = a_q e^{-jb_q}$ where $a_q = |h_q|$ and b_q is the phase of h_q such that $E(a_q) = \frac{\sqrt{\pi}}{2\sqrt{D_2^{ple}}}$ and $E(a_q^2) = E(|h_q|^2) = \frac{1}{D_2^{ple}}$ [25]. We have $g_q = c_q e^{-jd_q}$ such that $E(c_q) = \frac{\sqrt{\pi}}{2\sqrt{D_3^{ple}}}$ and $E(c_q^2) = E(|g_q|^2) = \frac{1}{D_3^{ple}}$.

The phase of q-th reflector is [1]

$$\phi_q = b_q + d_q. \quad (3)$$

The received signal S_D is written as

$$r_p = s_p \sqrt{E_{BS}} \sum_{q=1}^{N} h_q g_q e^{j\phi_q} + n_p. \quad (4)$$

where s_p is the p-th transmitted symbol and n_p is a Gaussian noise of variance N_0.

Using (3), we obtain

$$r_p = s_p \sqrt{E_{S_S}} \sum_{q=1}^{N} a_q c_q + n_p. \quad (5)$$

The signal-to-noise ratio (SNR) at S_D is written as [1]

$$\gamma^{S_D} = \frac{E_{S_S}}{N_0} [\sum_{q=1}^{N} a_q c_q]^2, \quad (6)$$

Using (2), we obtain

$$\gamma^{S_D} = \frac{\mu a E_A}{(1-a)(1-b)N_0} \sum_{l=1}^{n_r} |f_l|^2 [\sum_{q=1}^{N} a_q c_q]^2, \quad (7)$$

For a large number of reflectors, i.e., $N \geq 8$, $\sum_{q=1}^{N} a_q c_q$ follows a Gaussian distribution with mean $m = \frac{N\pi}{4\sqrt{D_2^{ple} D_3^{ple}}}$ and variance $\sigma^2 = \frac{N}{D_2^{ple} D_3^{ple}} [1 - \frac{\pi^2}{16}]$. As $[\sum_{q=1}^{N} a_q c_q]^2$ is non-central Chi-square r.v. and $\sum_{l=1}^{n_r}|f_l|^2$ is a central chi-square r.v, the probability density function (PDF) of γ^{S_D} is written as [22]

$$\begin{aligned} p_{\gamma^{S_D}}(x) = & \frac{N_0(1-a)(1-b)e^{-0.5(\frac{m}{\sigma})^2}D_1^{ple}}{\mu a E_A \Gamma(n_r)} \\ & \times \sum_{q=0}^{+\infty} \frac{(\frac{m}{\sigma})^{2q} 2^{\frac{-3q-n_r+1.5}{2}}}{q!\Gamma(q+0.5)} \\ & \times K_{q-n_r+0.5}(\sqrt{\frac{2xD_1^{ple}N_0(1-a)(1-b)}{a\mu E_A}}) \\ & \times (\frac{xD_1^{ple}N_0(1-a)(1-b)}{\mu a E_A})^{\frac{q+n_r-1.5}{2}} \end{aligned} \quad (8)$$

We use [23]

$$\begin{aligned} & \int_0^y \frac{2(CD)^{0.5C+0.5D}}{\Gamma(C)\Gamma(D)} x^{0.5C+0.5D-1} K_{C-D}(2\sqrt{CDx})dx \\ & = \frac{1}{\Gamma(C)\Gamma(D)} G_{1,3}^{2,1}\left(CDy|_{C,\ D,\ 0}^{1}\right) \end{aligned} \quad (9)$$

to obtain

$$\int_0^{\sqrt{x}} w^{C-1}K_D(w)dw = 2^{C-2}G_{1,3}^{2,1}\left(\frac{x}{4}|_{\frac{C+D}{2},\ \frac{C-D}{2},\ 0}^{1}\right) \quad (10)$$

where $G_{n,m}^{p,l}(x)$ is the Meijer G-function.

We deduce the cumulative distribution function (CDF) of γ^{S_D}:

$$\begin{aligned} & P_{\gamma^{S_D}}(x) \\ & = \frac{e^{-(\frac{m}{\sqrt{2}\sigma})^2}}{\Gamma(n_r)} \sum_{p=0}^{+\infty} \frac{(\frac{m}{\sigma})^{2p}2^{-p}}{p!\Gamma(p+0.5)} \\ & \times G_{1,3}^{2,1}\left(\frac{N_0(1-a)(1-b)xD_1^{ple}}{2\mu a E_A}|_{p+0.5,\ n_r,\ 0}^{1}\right) \end{aligned} \quad (11)$$

The packet error probability (PEP) at S_D can be computed as [24]

$$PEP(a,b) < P_{\gamma^{S_D}}(W_0) \quad (12)$$

where W_0 is defined as [24]

$$W_0 = \int_0^{+\infty} pep(v)dv \quad (13)$$

$pep(v)$ is the PEP for for Q-QAM modulation [25]

$$\begin{aligned} & pep(v) \\ & = 1 - \left[1 - 2\left(1 - \frac{1}{\sqrt{Q}}\right) erfc\left(\sqrt{v\frac{3\log_2(Q)}{2(Q-1)}}\right)\right]^{PL} \end{aligned} \quad (14)$$

and PL is packet length in symbols.

The throughput at S_D is computed as

$$\begin{aligned} Thr(a,b) = & \frac{(1-b)(1-a)L_0 log_2(Q)}{L_0 T_s B} \\ & \times(1-PEP(a,b))P_{idle}(1-P_f(a,b)) \\ = & (1-b)(1-a)log_2(Q) \\ & \times(1-PEP(a,b))P_{idle}(1-P_f(a,b)) \end{aligned} \quad (15)$$

where B is the used bandwidth, $P_f(a,b)$ is the false alarm probability written as

$$P_f(a,b) = \frac{\Gamma(\lfloor(1-a)bL_0\rfloor, \frac{\zeta}{2})}{\Gamma(\lfloor(1-a)bL_0\rfloor)} \quad (16)$$

ζ is the energy detector threshold, $\lfloor(1-a)bL_0\rfloor$ is the number of samples employed by the energy detector, and $\lfloor x\rfloor$ is the integer part of x,

$$\Gamma(N,u) = \int_u^{+\infty} x^{N-1}e^{-x}dx. \quad (17)$$

Harvesting duration a and sensing duration b are optimized to maximize the throughput:

$$(a_{opt}, b_{opt}) = argmax_{a,b} Thr(a,b) \quad (18)$$

3 CRN using two IRS

Figure 2 depicts a system model containing two IRS: IRS_1 is used for increase the harvested energy with N_1 reflectors . IRS_1 is between A and S_S to increase the harvested energy. IRS_2 is located between S_S and S_D; it contains N_2 reflectors to increase the SNR at S_D.

When IRS_1 is used, the harvested energy is equal to

$$E = \mu a L_0 E_A[\sum_{l=1}^{N_1}\delta_l\eta_l]^2, \quad (19)$$

$\delta_l = |u_l|$, where u_l is channel gain between A and l-th reflector of IRS_1, and $\eta_l = |v_l|$ where v_l is the channel gain between l-th reflector of IRS_1 and S_S.

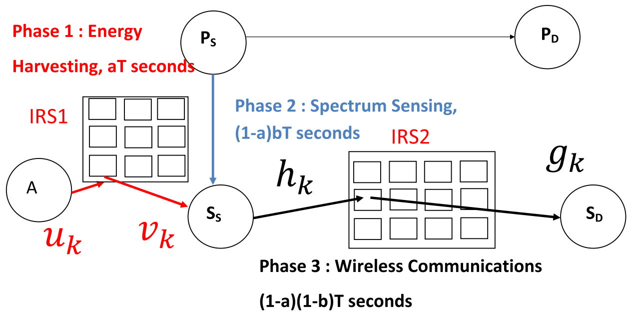

Fig. 2 IRS using in energy harvesting

For large values of $N_1 \geq 8$, $[\sum_{l=1}^{N_1} \delta_l \eta_l]$ follows a Gaussian distribution with mean $m_2 = \frac{N_1 \pi}{4\sqrt{D_4^{ple} D_5^{ple}}}$ and variance $\sigma_2^2 = \frac{N_1}{D_4^{ple} D_5^{ple}}$. D_4 is the distance between A and IRS_1, and D_5 is the distance between IRS_1 and S_S.
We can write

$$E_{S_D} = \frac{E}{L_0(1-a)(1-b)} = \frac{\mu a E_A[\sum_{l=1}^{N_1} \delta_l \eta_l]^2}{(1-a)(1-b)} \tag{20}$$

The SNR at S_D is equal to

$$\gamma^{S_D} = \frac{E_{S_S}[\sum_{q=1}^{N_2} a_q c_q]^2}{N_0} = \frac{\mu a E_A}{N_0(1-a)(1-b)}[\sum_{l=1}^{N_1} \delta_l \eta_l]^2[\sum_{q=1}^{N_2} a_q c_q]^2. \tag{21}$$

where a_q, c_q were defined in Sect. 2 and N_2 is the number of reflectors of IRS_2.

As $[\sum_{l=1}^{N_1} \delta_l \eta_l]^2$ and $[\sum_{q=1}^{N_2} a_q c_q]^2$ are two non-Chi-square r.v., the PDF of γ^{S_D} is written as [22]

$$f_{\gamma^{S_D}}(z) = e^{-\frac{m_2^2}{2\sigma_2^2}-\frac{m_4^2}{2\sigma_3^2}} \sum_{n=0}^{+\infty}\sum_{p=0}^{+\infty} \frac{2^{-2n-2p}(\frac{m_2}{\sigma_2})^{2p}(\frac{m_4}{\sigma_3})^{2n}}{n!p!\Gamma(n+0.5)\Gamma(p+0.5)} \times \frac{N_0(1-a)(1-b)}{\mu a E_A} K_{p-n}(\sqrt{\frac{N_0(1-a)z}{\mu a E_A}}) \times (z\frac{N_0(1-a)(1-b)}{\mu a E_A})^{\frac{p+n-1}{2}} \tag{22}$$

Using (10), the CDF of γ^{S_D} is equal to

$$P_{\gamma^{S_D}}(z) = e^{-\frac{m_2^2}{2\sigma_2^2}-\frac{m_3^2}{2\sigma_3^2}} \sum_{n=0}^{+\infty}\sum_{p=0}^{+\infty} \frac{2^{-n-p}(\frac{m_2}{2\sigma_2})^{2p}(\frac{m_3}{2\sigma_3})^{2n}}{n!p!\Gamma(n+0.5)\Gamma(p+0.5)} \times G_{1,3}^{2,1}\left(\frac{N_0(1-a)(1-b)z}{\mu a E_A 4} \middle| \begin{matrix} 1 \\ p+0.5,\ n+0.5,\ 0 \end{matrix}\right) \tag{23}$$

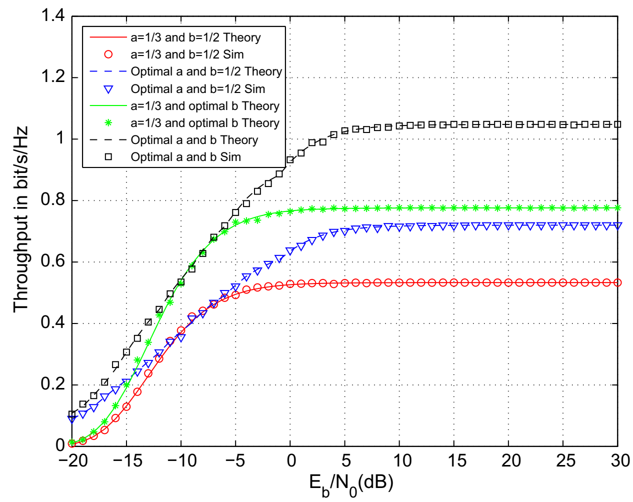

Fig. 3 Throughput for QPSK and one IRS

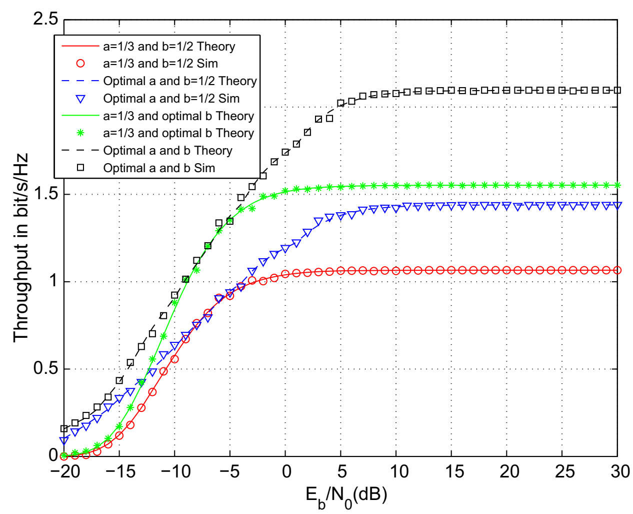

Fig. 4 Throughput for 16QAM and one IRS

where $m_3 = \frac{N_2^2 \pi}{4\sqrt{D_2^{ple} D_3^{ple}}}$, $\sigma_3^2 = \frac{N_2^2}{D_2^{ple} D_3^{ple}}[1 - \frac{\pi^2}{16}]$.

The throughput is computed and optimized using (12-18).

4 Numerical results

Figures 3, 4 and 5 depicts the throughput for QPSK, 16 and 64 QAM modulation in the presence of one IRS with $M = 8$ reflectors for $\zeta = 1$, $D_1 = 1$, $D_2 = 1.3$, $D_3 = 1.4$, $E_A = 1$. We notice that the optimization of harvesting and sensing duration offers the largest throughput when compared to $a = 1/3$, $b = 1/2$, optimal a, $b = 1/2$ and optimal b with $a = 1/3$.

For the same parameters as Figs. 3, 4 and 5, Figures 6 and 7 show the throughput for 16 and 64 QAM modulations and different number of reflectors $N = 8, 16, 32, 64, 128, 256, 512$.

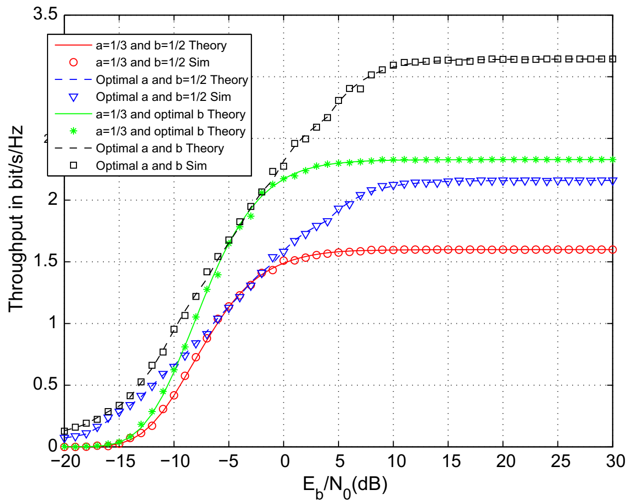

Fig. 5 Throughput for 64QAM and one IRS

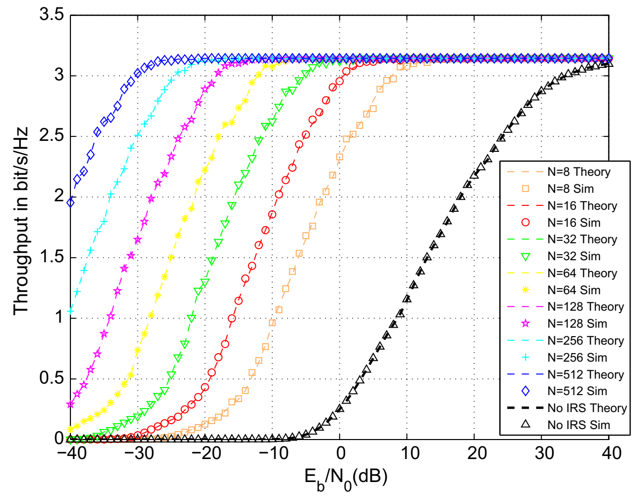

Fig. 7 Throughput for 64QAM and different number of reflectors

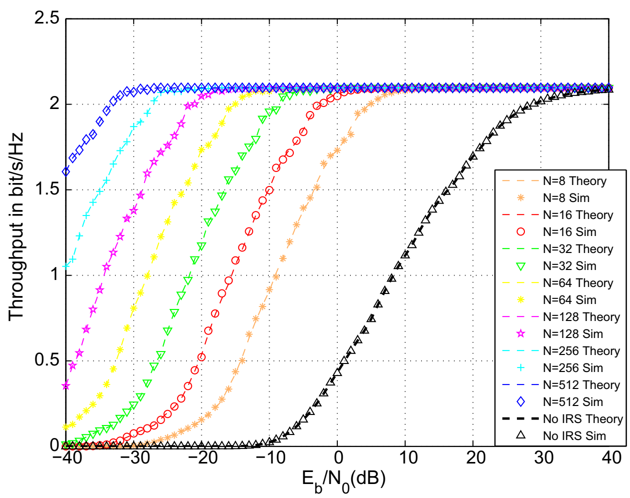

Fig. 6 Throughput for 16QAM with different number of IRS reflectors

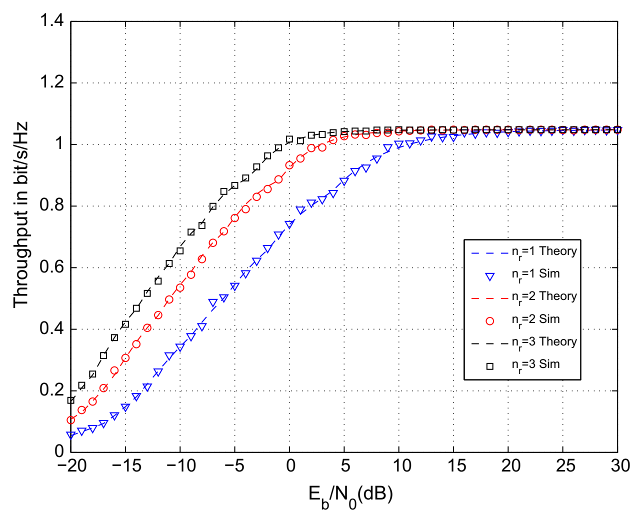

Fig. 8 Throughput for QPSK and different number of harvesting antennas

The use of $N = 8, 16, 32, 64, 128, 256, 512$ reflectors offers 19, 25, 31, 37, 43, 49, 56 dB gain when compared to the absence of IRS [20]. In Fig. 6-7, we used an optimal value of a and b.

Figure 8 shows the effect of number of harvesting antennas $n_r = 1, 2, 3$ on secondary throughput for QPSK modulation, $N = 8$ reflectors and the same parameters as Fig. 3. We notice that $n_r = 3$ harvesting antennas offers 2 dB and 7 dB gain when compared to $n_r = 2, 1$.

Figure 9 depict the throughput for QPSK modulation when there are two IRS with $D_4 = 1.1$ and $D_5 = 1.2$. The other parameters are the same as Fig. 3. The use of two IRS with $N_1 = 8$ reflectors in the first IRS and $N_2 = 8$ reflectors in the second IRS offers 12 dB and 30 dB gain when compared to a single IRS $N = 8$ and the absence of IRS [20]. The use of two IRS with $N_1 = 16$ and $N_2 = 8$ offers 21 dB and 39 dB gain when compared to a single IRS $N = 8$ and the absence of IRS [20].

5 Conclusion and perspectives

In this article, we optimized harvesting and sensing duration for CRN using intelligent reflecting surfaces (IRS). IRS reflects signals from secondary source so that all reflections are in phase at secondary destination. The use of $N = 8, 16, 32, 64, 128, 256, 512$ reflectors offers 19, 25, 31, 37, 43, 49, 56 dB gain when compared to the absence of IRS [20]. We also proposed to add a second IRS to increase the harvested energy where the secondary source harvests energy using the reflected signals on the first IRS. The use of two IRS with $N_1 = 8$ reflectors in the first IRS and $N_2 = 8$

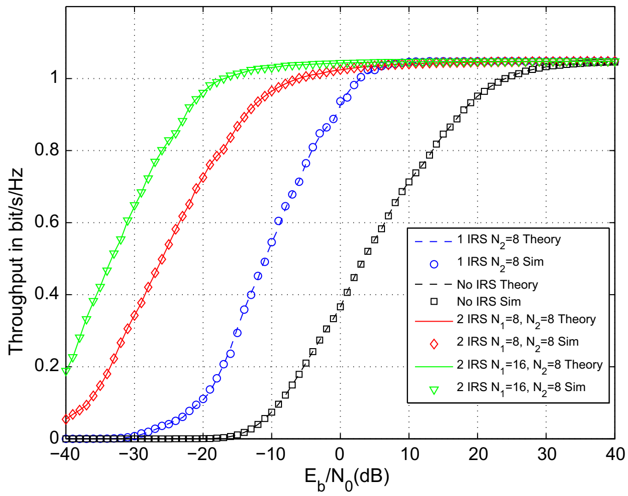

Fig. 9 Throughput for QPSK with two IRS

reflectors in the second IRS offers 12 dB and 30 dB gain when compared to a single IRS $N = 8$ and the absence of IRS [20]. The use of two IRS with $N_1 = 16$ and $N_2 = 8$ offers 21 dB and 39 dB gain when compared to a single IRS $N = 8$ and the absence of IRS [20]. As a perspective, we may extend the system model to NOMA systems.

References

1. Basar, E., Di Renzo, M., De Rosny, J., Debbah, M., Alouini, M.S., Zhang, R.: Wireless Communications Through Reconfigurable Intelligent Surfaces. IEEE Access **7**, 116753–116773 (2019)
2. Zhang, H., Di, B., Song, L. and Han, Z.: Reconfigurable Intelligent Surfaces Assisted Communications With Limited Phase Shifts: How Many Phase Shifts Are Enough?. IEEE Trans. Vehicular Technol. 69: 4498-4502.(2020)
3. Di Renzo, M: 6G Wireless: Wireless Networks Empowered by Reconfigurable Intelligent Surfaces. 2019 25th Asia-Pacific Conference on Communications (APCC)
4. Basar, Ertugrul: "Reconfigurable Intelligent Surface-Based Index Modulation: A New Beyond MIMO Paradigm for 6G", IEEE Transactions on Communications, Early Access Article, (2020)
5. Wu, Q., Zhang, R: Towards smart and reconfigurable environment: intelligent reflecting surface aided wireless network. IEEE Commun. Magazine, 58 (2020)
6. Huang, C., Zappone, A., Alexandropoulos, G.C., Debbah, M. and Yuen, C.: Reconfigurable intelligent surfaces for energy efficiency in wireless communication. IEEE Trans. Wireless Commu., 18, 4157-4170. (2019)
7. Alexandropoulos, G.C. and Vlachos, E.: A hardware architecture for reconfigurable intelligent surfaces with minimal active elements for explicit channel estimation. ICASSP 2020 - 2020 IEEE International Conference on Acoustics, Speech and Signal Processing (ICASSP), (2020)
8. Guo, H., Liang, Y.C., Chen, J., Larsson, E.G.: Weighted sum-rate maximization for reconfigurable intelligent surface aided wireless network. IEEE Trans. Wireless Commun. 19, 3064-3076 (2020)
9. Thirumavalavan, V.C. and Jayaraman, T.S.: BER analysis of reconfigurable intelligent surface assisted downlink power domain NOMA system. 2020 International Conference on COMmunication Systems and NETworkS (COMSNETS), (2020)
10. Yang, L., Guo, W. and Ansari, I.S: Mixed dual-hop FSO-RF communication systems through reconfigurable intelligent surface. IEEE Commun. Lett. Early Access Article, (2020)
11. Pradhan, C., Li, A., Song, L., Vucetic, B. and Li, Y.: Hybrid precoding design for reconfigurable intelligent surface aided mmWave communication systems. IEEE Wireless Commun. Lett. 9(7), 1041-1045. (2020)
12. Ying, K., Gao, Z., Lyu, S., Wu, Y., Wang, H. and Alouini, M.S.: GMD-based hybrid beamforming for large reconfigurable intelligent surface assisted millimeter-wave massive MIMO, IEEE Access, 8, 19530-19539. (2020)
13. Di, B., Zhang, H., Li, L., Song, L., Li, Y. and Han, Z.: Practical hybrid beamforming with finite-resolution phase shifters for reconfigurable intelligent surface based multi-user communications. IEEE Trans. Vehicular Technol. 69(4), 4565-4570. (2020)
14. Kammoun, A., Chaaban, A., Debbah, M. and Alouini, M.S.: Asymptotic max-min SINR analysis of reconfigurable intelligent surface assisted MISO systems. . IEEE Transactions on Wireless Communication 19, 7748-7764 (2020)
15. Zhao, W., Wang, G., Atapattu, S., Tsiftsis, T.A. and Tellambura, C.: Is backscatter link stronger than direct link in reconfigurable intelligent surface-assisted system?. IEEE Commun. Lett. 24, 1342-1346. (2020)
16. Li, S., Duo, B., Yuan, X., Liang, Y.C. and Di Renzo, M.: Reconfigurable intelligent surface assisted UAV communication: Joint trajectory design and passive beamforming. IEEE Wireless Commun. Lett. 9, 716-720.(2020)
17. Dai, L., Wang, B., Wang, M., Yang, X., Tan, J., Bi, S., Xu, S., Yang, F., Chen, Z., Di Renzo, M. and Chae, C.B.: Reconfigurable intelligent surface-based wireless communications: Antenna design, prototyping, and experimental results. IEEE Access, 8, 45913-45923. (2020)
18. Hua, S., Shi, Y.: Reconfigurable intelligent surface for green edge inference in machine learning. 2019 IEEE Globecom Workshops (GC Wkshps), (2019)
19. Huang, C., Alexandropoulos, G.C., Yuen, C. and Debbah, M.: Indoor signal focusing with deep learning designed reconfigurable intelligent surfaces. 2019 IEEE 20th International Workshop on Signal Processing Advances in Wireless Communications (SPAWC), (2019)
20. Raed Alhamad, Hatem Boujemaa, "Optimal harvesting and sensing durations for cognitive radio networks", Signal Image Video Process. 14(7), 1397–1404 (2020)
21. Alhamad, R.:Non orthogonal multiple access with adaptive transmit power and energy harvesting using intelligent reflecting surfaces for cognitive radio networks. Submitted to Signal Image Video Process, (2021)
22. Wells, W.T., Anderson, R. L., Cell, John W.: The Distribution of the Product of Two Central or Non-Central Chi-Square Variates. Ann. Math. Statistics **33**(3), 1016–1020 (1962)
23. Marzieh Najafi, Vahid Jamali, Panagiotis D. Diamantoulakis, George K. Karagiannidis and Robert Schober, "Non-Orthogonal Multiple Access for FSO Backhauling", IEEE WCNC, Barcelona 2018
24. Xi, Y., Burr, A., Wei, J.B., Grace, D.: A general upper bound to evaluate packet error rate over quasi-static fading channels. IEEE Trans. Wireless Communications **10**(5), 1373–1377 (2011)
25. Proakis, J.: Digital Communications, 5th edn. Mac Graw-Hill (2007)